Oecologia
https://doi.org/10.1007/s00442-019-04550-6

GLOBAL CHANGE ECOLOGY – ORIGINAL RESEARCH

# Recent increases in drought frequency cause observed multi-year drought legacies in the tree rings of semi-arid forests

**Paul Szejner**[1,2] · **Soumaya Belmecheri**[1] · **James R. Ehleringer**[3] · **Russell K. Monson**[1,4]

Received: 3 May 2019 / Accepted: 29 October 2019


## Abstract

Recent analyses on the length of drought recovery in forests have shown multi-year legacies, particularly in semi-arid, coniferous ecosystems. Such legacies are usually attributed to ecophysiological memory, although drought frequency itself, and its effect on overlapping recovery times, could also contribute. Here, we describe a multi-decadal study of drought legacies using tree-ring carbon-isotope ratios ($\delta^{13}C$) and ring-width index (RWI) in *Pinus ponderosa* at 13 montane sites traversing a winter–summer precipitation gradient in the Southwestern U.S. Sites and trees were selected to avoid collection biases that exist in archived tree-ring databanks. The spatial hydroclimate gradient and winter–summer seasonal patterns were well predicted by seasonal and inter-annual correlations between $\delta^{13}C$ and atmospheric vapor pressure deficit (VPD). Using VPD, we found that the probability of extreme drought has increased up to 70% in this region during the past two decades. When the recent increase in drought frequency was not considered, multi-year legacies in both $\delta^{13}C$ and RWI were observed at most sites. When the increase in drought frequency was detrended from tree-ring chronologies, some sites exhibited short legacies (1–2 years) in both $\delta^{13}C$ and RWI, and there was a sight trend for longer legacies in RWI. However, when considered broadly across the region and multiple decades, no significant legacies were observed, which contrasts with past studies. Our results reveal that a contribution to observed multi-year legacies is related to shifts in the climate system itself, an exogenous factor, that must be considered along with physiological memory.

**Keywords** Pulse–press disturbance · Xylem vulnerability · Stress recovery · Stress memory · Hot droughts · Climate change · Vapor pressure deficit · Modeling

## Introduction

While trends in the intensity and areal coverage of droughts over the past century are uncertain (Dai et al. 2004; Huntington 2006; Sheffield et al. 2012; Dai 2013; Trenberth et al. 2014; Prein et al. 2016), continued climate warming will most likely cause increased drought in both of these dimensions, especially in semi-arid and arid regions (Cook et al. 2015; Touma et al. 2015). Greater drought stress would compromise the capacity of global ecosystems to sequester carbon from the atmosphere (Anderegg et al. 2015; Schwalm et al. 2017; Mekonnen et al. 2017) and potentially enhance positive climate feedbacks leading to even greater warming (Stark et al. 2016). Regional changes in precipitation and humidity are expected to amplify historical trends, causing drier regions to get drier and wetter regions to get wetter, posing an external threat to already vulnerable water-limited forest ecosystems (Williams et al. 2013; Trenberth et al. 2014; Ficklin and Novick 2017; Dorado-Liñán et al. 2019).

Communicated by Arthur Gessler.

**Electronic supplementary material** The online version of this article (https://doi.org/10.1007/s00442-019-04550-6) contains supplementary material, which is available to authorized users.

✉ Paul Szejner
paulszejner@email.arizona.edu

[1] Laboratory of Tree-Ring Research, University of Arizona, 1215 E Lowell St, Tucson, AZ 85721, USA

[2] School of Natural Resources and the Environment, University of Arizona, 1064 E. Lowell St., Tucson, AZ 85721, USA

[3] Department of Biology, University of Utah, Salt Lake City, UT 84112, USA

[4] Department of Ecology and Evolutionary Biology, University of Arizona, Tucson, AZ 85721, USA

Published online: 04 November 2019

Recent model projections indicate that the Southwestern U.S. (hereafter SW) will experience more frequent and hotter droughts (Seager et al. 2013; Ault et al. 2016; Prein et al. 2016), which have been linked to structural changes in forested ecosystems and mass mortality of trees (McDowell et al. 2015; Allen et al. 2015; Hartmann et al. 2018). Uncertainties in the magnitude, frequency and impact of droughts will challenge our ability to accurately predict changes in regional-to-global carbon and water cycles (Poulter et al. 2014; Anderegg et al. 2015; Biederman et al. 2017; Kolus et al. 2019; Pugh et al. 2019).

Recently, research has focused on persistent, multi-year influences of droughts on forest tree growth—so-called drought legacy effects (Reichstein et al. 2013; Anderegg et al. 2015; Ogle et al. 2015; Peltier et al. 2016; Schwalm et al. 2017; Kannenberg et al. 2019a, b; Peltier and Ogle 2019a). Studies using multi-decadal tree-ring width indices (RWI) have suggested that the impact of extreme drought on net primary productivity (NPP) can last up to several years and that the impacts are greatest in semi-arid needleleaf forests in the Northern Hemisphere (Anderegg et al. 2015; Peltier et al. 2016; Wu et al. 2017; Peltier and Ogle 2019a). One factor that has not received adequate attention in characterizing post-drought legacies is the potential for a change in the frequency of drought events themselves; that is, a climate effect on drought legacies, as an additive or synergistic influence on ecophysiological memory (Kannenberg et al. 2019a; Peltier and Ogle 2019b). In several past studies, legacy causes have been attributed to both exogenous (e.g., abiotic) and endogenous (e.g., physiological) factors, with most attention given to the latter (Barron-Gafford et al. 2014; Anderegg et al. 2015; Ogle et al. 2015; Peltier et al. 2016, 2017; Peltier and Ogle 2019a). Endogenous factors include limitations in the availability of non-structural carbohydrate (NSC) reserves that maintain turgor pressure and sustain recovery processes following stress (Hacke et al. 2001; Timofeeva et al. 2017; Adams et al. 2017; Schönbeck et al. 2018; Peltier and Ogle 2019a), pre-drought photosynthetic potential (Barron-Gafford et al. 2014), growth potential (Lloret et al. 2011; Peltier et al. 2016), hysteresis in stomatal conductance (Powell et al. 2013; Ogle et al. 2015), and biomass allocation limitations in the capacity for trees to construct leaves, xylem and fine roots following drought (Farrior et al. 2013; Powell et al. 2013). All of these effects might cause reduced growth in the immediate years following a drought, producing a drought 'memory'. Abiotic exogenous factors, such as the frequency of drought events, can directly influence the span of drought memory, especially when the effects of the events overlap in time. The influences of increased drought frequency on ecophysiological memory can potentially amplify negative carbon balances and push forest ecosystems past thresholds of sustainability (Sevanto et al. 2014; Serra-Maluquer et al. 2018; Peltier and Ogle 2019a). These effects on the forests can result in progressive declines in tree fitness, cascading patterns of mass tree mortality, and the establishment of novel ecosystem states (Breshears et al. 2005; McDowell et al. 2015; Allen et al. 2015; Hartmann et al. 2018; Hammond et al. 2019). These effects are especially important in the southwestern US, the region that serves as the focus of this study.

We conducted observations of cellulose carbon-isotope ratios ($\delta^{13}C$) and ring-width indices (RWI), seasonally resolved with respect to spring and summer, in the earlywood and latewood of *Pinus ponderosa* (Douglas ex C. Lawson) trees from 13 montane forests to gain an understanding of the causes and patterns of drought-related legacies. Carbon-isotope ratios provided an integrated assessment of multiple interacting influences of drought on tree carbon assimilation and water use. Tree-ring width analyses provided us with a relative and time-integrated metric of aboveground growth and NPP (Kozlowski et al. 1991; Babst et al. 2014). Past studies have shown a positive correlation between $\delta^{13}C$ and RWI that is consistent with a correlated effect of drought on both the physiological determinants of leaf-scale fractionation and woody biomass increase (Francey and Farquhar 1982). We used the theoretical and observational support for these correlations as justification to examine patterns in both $\delta^{13}C$ and RWI, and as a means to evaluate both endogenous and exogenous components of drought legacies. The study region that we chose includes a latitudinal gradient in the relative abundances of winter–spring versus summer precipitation, but with similar montane vegetation, community structure and species composition. We chose to focus on *Pinus ponderosa* because it is the dominant tree species of most montane, mid-elevation forests in the Western U.S. Our analysis differs from those in many past studies of drought legacies in that we: (1) chose sites and trees to provide systematic coverage across a broad latitudinal precipitation gradient, rather than relying on archived samples in the International Tree-Ring Data Base (ITRDB) or collections made across sites with similar climatology, (2) assessed seasonal patterns in tree-ring earlywood and latewood growth components (EW and LW, respectively) and precipitation, rather than relying on integrated annual growth increments, (3) developed a stable-isotope analysis to complement the traditional approach of using RWIs, and (4) applied an analytical framework that extended further into the initial two decades of the twenty-first century than those from past studies, and therefore had greater potential to detect the most recent trends in regional climate and their effect on tree responses. We hypothesized that evidence of multi-year drought legacies would be present in the observations of both EW and LW $\delta^{13}C$ and RWI and that the length of individual legacies would be, at least partly, dependent on the frequency of subsequent droughts, following an extreme event.

## Methods

### Overall approach

We used a network of sites within the geographic domain of the North American Monsoon (NAM) climate system (Fig. 1). At each site, tree cores from *P. ponderosa* trees were used to construct EW and LW chronologies of $\delta^{13}C$ and RWI. The sites and sampled trees were selected using the following criteria (also see Szejner et al. 2016): (1) exclusion of sites with large surrounding watersheds that could contribute runoff water; (2) selection of medium-aged trees (e.g., 100–250 years); (3) selection of sites with evidence of low tree-to-tree canopy competition, and no evidence of past-century land-use change; (4) selection of trees that showed signs of vigorous recent growth with a well-formed and symmetrical crown. We studied the temporal variations in RWI and $\delta^{13}C$ from extracted α-cellulose, using EW as a spring proxy and LW, as a summer proxy.

### Stable-isotope analysis and ring-width analysis

We used 2–3 combined, 5-mm diameter cores from five trees at each site for isotope analysis, and single cores from 5 to

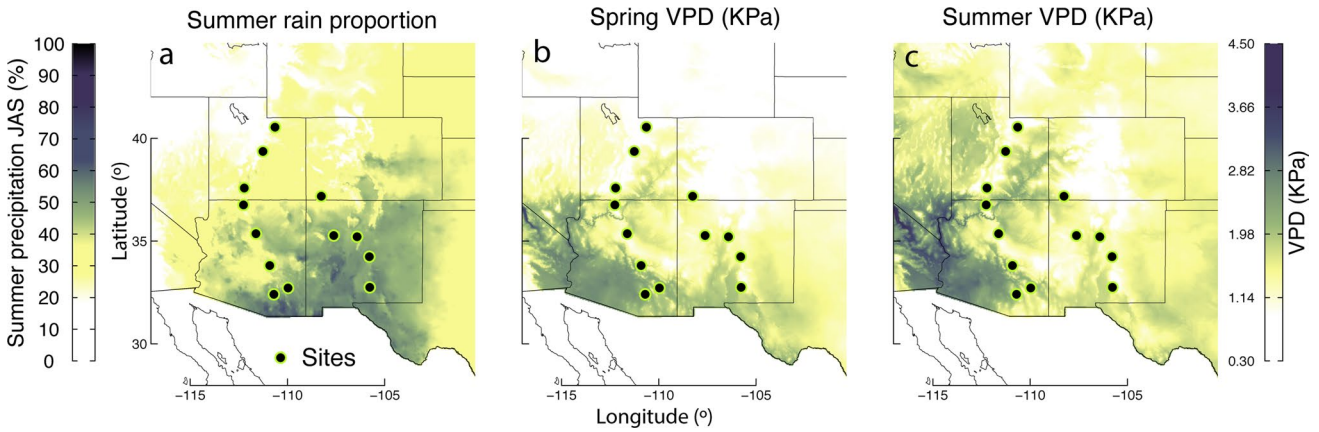


**Fig. 1** Tree-ring network and associated seasonal hydroclimate regime. **a** Site locations on a map of the summer (June, August, September) rain-percentage of total annual precipitation. **b** Daily-averaged mean spring (AMJ) VPD (kPa). **c** Daily-averaged mean summer (JAS) VPD (kPa). Values are mapped at 4-km resolution

**Table 1** Sites used in the study, including codes used in the text, locations, elevations, measures of variability for the RWI observations and number (*N*) of tree measured for RWI

| Site | Code | Long (E°) | Lat (N°) | Elevation (masl) | Isotope chronology span (years) | RWI rbar | RWI EPS | N trees measured for RWI |
|---|---|---|---|---|---|---|---|---|
| Santa Catalina Mountains (AZ) | WCP | − 110.70 | 32.41 | 2317 | 80 | 0.537 | 0.839 | 8 |
| Pinaleño Mountains (AZ) | CPP | − 109.97 | 32.72 | 2682 | 53 | 0.623 | 0.889 | 9 |
| Sacramento Mountains (NM) | SLS | − 105.77 | 32.75 | 2551 | 53 | 0.37 | 0.865 | 13 |
| Sierra Ancha (AZ) | SAP | − 110.91 | 33.81 | 2218 | 53 | 0.35 | 0.655 | 5 |
| Gallinas Mountains (NM) | GHP | − 105.79 | 34.24 | 2426 | 53 | 0.863 | 0.959 | 5 |
| Sandia Mountains (NM) | SPP | − 106.42 | 35.21 | 2716 | 53 | 0.585 | 0.849 | 5 |
| Mt Taylor (NM) | CDT | − 107.62 | 35.27 | 2767 | 53 | 0.671 | 0.903 | 5 |
| Lockett Meadow (AZ) | LMP | − 111.62 | 35.36 | 2608 | 80 | 0.515 | 0.903 | 12 |
| Kaibab Plateau (AZ) | KPP | − 112.26 | 36.76 | 2271 | 53 | 0.637 | 0.968 | 29 |
| Mesa Verde (CO) | MVP | − 108.26 | 37.18 | 2767 | 102 | 0.446 | 0.861 | 18 |
| Bryce Canyon (UT) | BRY | − 112.22 | 37.58 | 2767 | 53 | 0.522 | 0.822 | 8 |
| Millers Flat (UT) | MFP | − 111.26 | 39.36 | 2435 | 53 | 0.685 | 0.951 | 21 |
| Rock Creek (UT) | RCP | − 110.64 | 40.54 | 2315 | 80 | 0.508 | 0.941 | 19 |

Sites are listed in latitudinal order from south-to-north (top-to-bottom)

*AZ* Arizona, *NM* New Mexico, *CO* Colorado, *UT* Utah

29 trees at each site for RWI analysis (Table 1). The cores were attached to wooden mounts using water-soluble hide glue. Each core was sanded with fine-grained sandpaper to allow for visual cross-dating (Stokes and Smiley 1996). After cross-dating, each annual ring intended for isotope analysis was sliced into three sections: EW, which was split into two halves EW1 and EW2, and LW. Sliced samples were ground to 20 mesh (0.84-mm particles) and heat sealed in permeable polymer-fabric bags (Ankom Technology, Macedon, NY, USA). Samples of α-cellulose were extracted from each sample following the method described by Leavitt and Danzer (1993), with the addition of a sodium hydroxide step, and additional modifications as described in Szejner et al. (2016). Only EW1 and LW were used for the isotopic analysis to ensure good seasonal separation of isotope signals. For each year that was analyzed, the samples from replicate cores of the same tree were combined; thus, allowing individual trees to serve as the fundamental statistical unit in all subsequent analyses. The coefficient of variation in $\delta^{13}C$ values among trees at each site, and averaged for all sites together, was 3.1 ± 0.7 (SD) % and 4.0 ± 1.2%, for EW and LW, respectively. Standard dendrochronological indices for variance among RWI samples are provided in Table 1.

The ratios of $^{13}C/^{12}C$ were measured from the $CO_2$ produced during α-cellulose combustion in a high-temperature conversion elemental analyzer coupled with a Thermo Delta Isotope Ratio Mass Spectrometer (TC/EA–IRMS) in the Environmental Isotope Laboratory of the Department of Geosciences at the University of Arizona. Isotope ratios are expressed in delta (δ) notation relative to the $\delta^{13}C$ of a Pee Dee Belemnite standard (in units of ‰). The $\delta^{13}C$ sample precision was calculated as ± 0.09 ‰. A correction to the isotope measurements was made to account for changes in the atmospheric $^{13}C/^{12}C$ ratio due to past-century fossil-fuel combustion (Suess 1955), and for the influence of progressive increases in atmospheric $CO_2$ on direct and indirect changes in the intercellular to ambient $CO_2$ concentration ($c_i/c_a$) (McCarroll et al. 2009).

Measurements of RWI were made to the nearest 0.001 mm using a Velmex TA linear encoder with Measure J2X software (VoorTech Consulting, Holderness, NH, USA). Each RWI series was detrended and standardized by fitting an exponential curve to remove age effects on the radial growth, followed by the calculation of RWI chronology means (Cook and Peters 1997) (Table 1).

Given our time and financial constraints, time-series for $\delta^{13}C$ was determined for the period 1960–2012 (53 years) at all sites, and for the period 1932–2012 (80 years) at three sites which were chosen to represent the endpoints and middle of the precipitation gradient (WCP, LMP, and RCP) (Fig. 1). For one site, the MVP site, we developed 102 years of $\delta^{13}C$ data (1911–2012). Thus, for four sites, we were able to extend the $\delta^{13}C$ time-series beyond the common all-site period of 53 years. For the RWI analyses, we used a time-series from 1900 to 2012 (113 years) at all sites. Chronologies for all sites are presented in time-series format in Figs. S1 and S2 in the Electronic Supplementary Materials.

## Seasonal climate signal from regional chronologies

Many of the $\delta^{13}C$ and RWI chronologies were observed to exhibit intra-annual cross-correlation between EW and LW. This cross-correlation is independent of climate variability and is potentially related to within-year utilization of common stored carbon or water pools (see analysis by Szejner et al. 2018). In these effects, it is the LW from a given year that carries the correlated signal associated with the preceding EW. To control for seasonal, cross-correlation, we estimated an adjusted-LW Index ($LW_{adj}$) for every year in the time series (Griffin et al. 2011; Szejner et al. 2018). The values of $LW_{adj}$ were defined from the residuals of a linear regression between each 'raw' LW and EW chronologies (Meko and Baisan 2001; Stahle et al. 2009; Griffin et al. 2011). The $LW_{adj}$ adjustment yields a new latewood chronology that is statistically independent of each year's preceding EW signal (Fig. S3 in Electronic Supplementary Materials).

In an initial analysis, we characterized regional coherence in chronologies using a principal component analysis (PCA) for the 53-year common period of 1960–2012 from all sites. The variables on each PCA were the 13 different chronologies using $\delta^{13}C$ and RWI for EW, and $LW_{adj}$ determined in separate analyses. The first principal components were expected to reveal the common temporal variability among sites as well as identify differences in the spatial distribution of its variance. The resultant time series or common temporal variability from the PCA (eigenvalues on each year) for EW and $LW_{adj}$ were compared with regionally gridded mean atmospheric water vapor pressure deficit (VPD, in kPa). Seasonal VPD was determined as the mean of daily averages, typically binned for spring-to-early summer (AMJ) or summer (JAS) months, using the Parameter-elevation Regressions on Independent Slopes Model (PRISM) climate dataset at 4-km resolution (PRISM Climate Group, Oregon State University, ver. 2004). To calculate daytime VPD, daily-averaged maximum temperatures were used to estimate the saturation vapor pressure ($e_s$) and dew-point temperatures were used to estimate the actual vapor pressure ($e_a$). We used April–June (AMJ), and July–September (JAS) mean VPD as the climate variables associated with the timing of formation and development of EW or $LW_{adj}$, respectively. These associations are based on identified correlations described previously (Szejner et al. 2016).

### Tree response to changes in drought frequency

To identify droughts, we applied the peak-over-threshold (POT) approach (Engeland et al. 2005) to determine those years that exceeded the 80th percentile of all monthly averaged seasonal mean VPDs within the timeframe 1900–2012. We focused on mean monthly atmospheric VPD as our measure of drought. This is justified by the fact that: (1) VPD limits surface conductance and evapotranspiration more than soil moisture in many temperate-latitude forests (Novick et al. 2016; Ficklin and Novick 2017), and (2) VPD has been identified as the factor most correlated with drought-associated declines in gross primary productivity (GPP) during the past 20 years (Yuan et al. 2019). Additionally, in this region, explicitly, the high correlation of oxygen- and carbon isotope enrichment with atmospheric humidity, precipitation and temperature has previously been established (Szejner et al. 2016). For further validation, we assessed the monthly correlation between PRISM VPD and SPEI (Standard Precipitation–Evapotranspiration Index) for every site and every month that we studied (Fig. S8 in Electronic Supplementary Materials). The correlation was generally greater than 0.85 and statistically significant ($P < 0.05$) at all but three winter periods for two of the northernmost sites.

For the $\delta^{13}C$ analysis, we only used droughts identified within the 53-year portion of the 80th-percentile time series that fell within the common interval of 1960–2012. For the RWI analysis, we used droughts derived from the entire 113-year length of the 80th-percentile time series. Each of the 13 sites was evaluated for their unique set of extreme drought years. Thus, we used ~ 10 extreme drought events per site for the $\delta^{13}C$ analysis of the sites with 53-year chronologies, ~ 16 extreme drought events for the three sites with 80-year chronologies, and ~ 20 drought events for the MVP site with the 102-year chronology. For the RWI analysis, we used ~ 22 extreme drought events per site for all sites. All drought events for all sites are reported in Fig. S4 of the Electronic Supplementary Materials.

For the $\delta^{13}C$ analysis, we partitioned the analysis according to the three distinct geographic regions initially identified in the PCA analysis (PC1-EW, PC1-$LW_{adj}$, and PC2-$LW_{adj}$), and for AMJ or JAS to provide the winter–spring (relevant to EW) and summer (relevant to $LW_{adj}$) seasonal mean VPDs. In one analysis (Fig. 2), a field correlation was constructed using the gridded geographic extent of PRISM-derived VPD in each of the three distinct PCA regions (initially determined by the correlation between $\delta^{13}C$ and VPD). The regional areal coverages of VPD for each of the three distinct PCA modes were computed using the average VPD of the 4 × 4 km grids in each PCA region that had correlation values higher than 0.65 ($P < 0.01$) between the entire time-series of the PCA correlation and the gridded time-series of PRISM-derived VPD.

To determine if the frequency of extreme droughts changed during the period of each chronology and the times series on for each PCA, the probability of occurrence in any given year was estimated using a Gaussian kernel along with a moving 30-year window (Mudelsee et al. 2003, 2004). The kernel-based estimation of event recurrence allows the detection of non-linear and non-monotonic frequency trends without imposing parametric restrictions. To account for error in the kernel estimates, we estimated 95% confidence intervals from 1000 bootstrapped, randomized resampling steps with the same number of drought events that were resolved in the original kernel estimate.

We also assessed temporal changes in the sensitivity of $\delta^{13}C$ and RWI independently in both EW and $LW_{adj}$ to a change in the frequency of winter–spring and summer drought events, respectively, using the full extent of each chronology (Table 1). A change in sensitivity was assessed through an examination of time-dependent trends in the variance and the correlation between $\delta^{13}C$ or RWI (for EW and $LW_{adj}$) with the corresponding seasonal VPD (AMJ or JAS). This assessment was conducted using a running window of 30 years. Temporal changes in variance and correlation trends were identified using a rank-based, non-parametric approach (Pettitt 1979). Using this method, we identified the timing of shifts in the variance or correlation time-series, which we interpret to reflect shifts in the sensitivity of $\delta^{13}C$ or RWI to a dynamic VPD time-series. We assume that an increase in the correlation of $\delta^{13}C$ or RWI to the time-dependent, back-and-forth VPD patterns of drought- and between-drought periods reveals an increased fidelity in the tracking of these ecophysiological indices with drought. Furthermore, the close tracking of $\delta^{13}C$ or RWI with VPD in a climate regime of increased fluctuation between drought and between-drought periods should be revealed in higher variance within the correlation. Together, the increase in correlation coefficients and variance should reveal higher sensitivity of the trees to a shift in fluctuating VPD dynamics. This concept of climate sensitivity is similar to, and based on the same statistical principle, as that from previous studies (Pedersen 1998; Ogle et al. 2000; McDowell et al. 2010; Lloret et al. 2011). Generally, in those studies, higher climate sensitivity was defined by a regression showing a steeper slope in the relation of RWI to progressive climate stress (Klesse et al. 2018).

### Assessing drought legacy effects

We applied the Superposed Epoch Analysis (SEA, see Chree 1913), from the R package Dendrochronology Program Library (dplR, Bunn 2008), to estimate the magnitude and duration of drought legacies. The SEA is a statistical

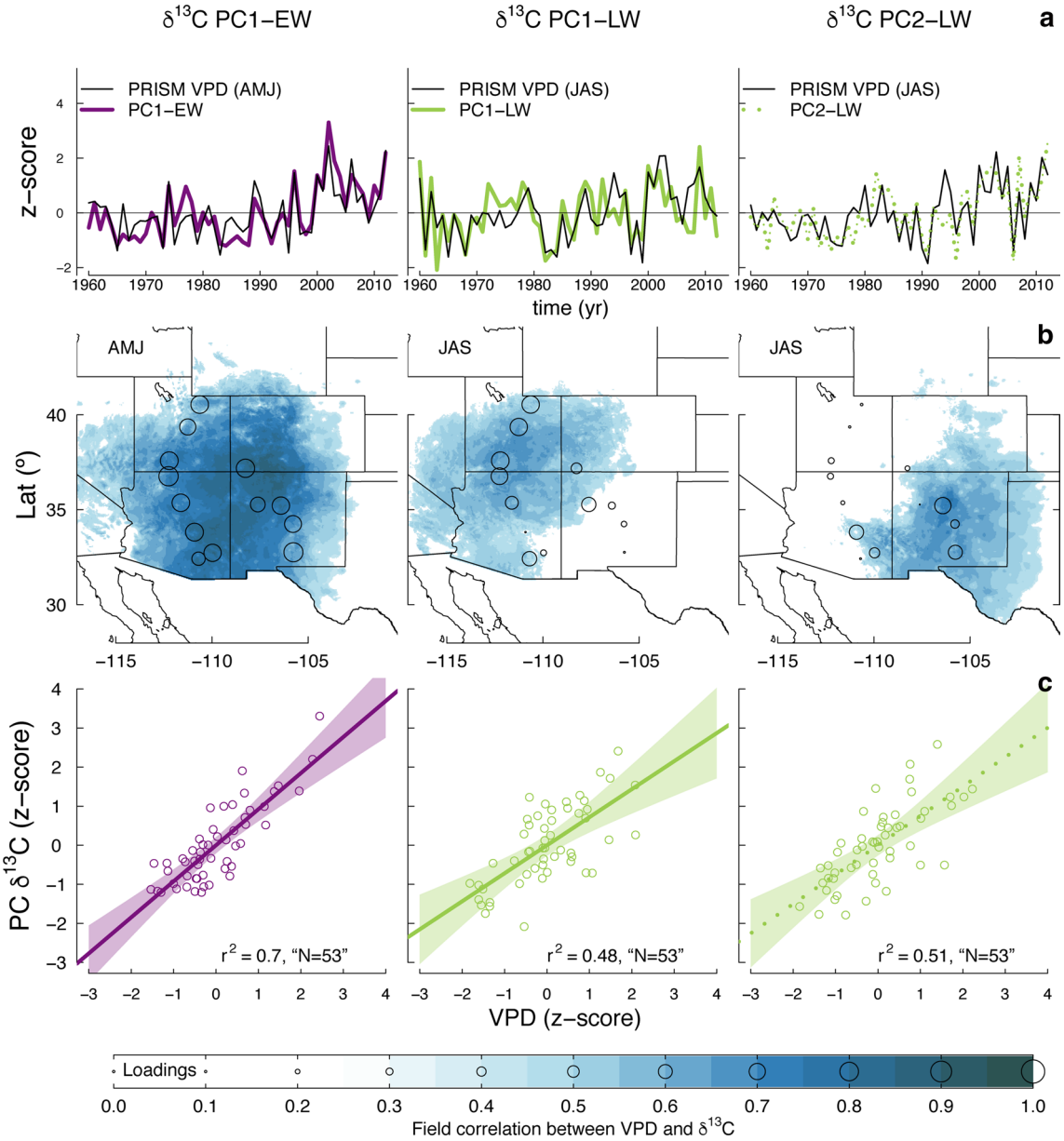


**Fig. 2** Principal component analysis (PCA) of $\delta^{13}C$ and regionally resolved VPD. Upper panels, Row **a** *z*-scores from the eigenvalues of each component (PC1-EW, PC1-$LW_{adj}$, and PC2-$LW_{adj}$), obtained from the computed correlation matrix of seasonal (AMJ or JAS) mean VPD against EW and $LW_{adj}$ $\delta^{13}C$ datasets. Middle panels, Row **b** Field correlation analysis between the 53-year PCA time series presented in Row **a**, and the 53-year PRISM time series of each 4° grid within each of the three PCA-resolved regions. Blue shading represents field correlations with $P \leq 0.01$, "$N=53$". The sizes of the black circles show the relative loadings for the PCA analysis at each of the 13 study sites. Lower panels, Row **c** Regression scatterplots showing the best-fit linear relationship between the 53-year averaged $\delta^{13}C$ and seasonal (AMJ or JAS) PRISM VPD, for each grid that showed an $r > 0.65$ in the field correlation analysis. Values used in the regressions are expressed as *z*-score deviations for each grid relative to the mean of all grids

technique intended to detect trends before, during and after specific key events in a time-series. Within our use of the SEA, "key events" were taken as analogous to "extreme drought events," which were identified through 80th-percentile VPD anomalies as described above. For each of the 13 study sites, we determined the mean standardized anomalies for $\delta^{13}C$ and RWI on each of the 1 year before each key event, the years of the key events, and each of the 5 years following each key event. Then, to asses, if the mean values in any preceding or succeeding year are significantly different from the average expectation, we applied SEA on a bootstrap resampling method based on 1000 randomly selected pseudo-key years from the chronologies (Haurwitz and Brier 1981).

The interpretation of the SEA can be biased if the temporal spacings between successive key events are distributed too close in time, producing an autocorrelation that crosses the span of the key events. In our analysis, if droughts are spaced too closely together, the effect of one drought can be carried into the occurrence of a subsequent drought, causing a time-dependent bias that might look like a persistent legacy effect. Our approach was to test for this type of cross-correlation bias, determine if it contributes to legacy effects and if so, remove the effect statistically. It is also possible for the analyzed time series to contain effects caused by processes that are not associated with the key drought events (Haurwitz and Brier 1981). To assess the potential for sequential correlation, trends and random-noise effects, we applied the SEA to four different versions of the $\delta^{13}C$ and RWI chronologies. We aimed to isolate the 'red-noise' form of the chronologies, which only retains the variability attributed to multi-year, cross-year autocorrelation in the absence of random (white noise) variance. It is the red-noise chronologies that we interpret as most revealing of potential post-drought legacies. The red-noise chronologies have the long-term systematic trend in drought removed, but retain the short-to-medium term stochastic trends that define legacy responses. To assess the legacies on these chronologies, we applied the SEA to the following versions of the time-series: (1) chronologies with any filtering; what we refer to as "raw chronologies", (2) raw chronologies that had been detrended using a 30-year spline to remove any long-term trends and multidecadal variability, thus retaining the variability related to medium- to short-term legacies, (3) chronologies with white noise removed (seasonal and interannual variance unrelated to the extreme events) to reveal only residual "red-noise chronologies", and (4) red-noise chronologies that were detrended using a 30-year spline. The detection of the white noise provided a 'working' chronology that was free of interannual autocorrelation. Then, this red-noise-free 'working' chronology was subtracted from the raw chronology revealing, as a residual, the ultimate red-noise chronology (which included the interannual autocorrelation). For the detrending procedures, we used the detrending functions in the Dendrochronology Program Library in R (dplR; Bunn 2008) using a 30-year smoothing spline to minimize any long-term trend in the chronology.

## Results

The 13 montane forest sites that were used in this study spanned a broad latitudinal gradient in the seasonal distribution of precipitation (Fig. 1). The sites in the northwestern part of the gradient receive most of their annual precipitation as snow or winter–spring rain, with a relatively dry mid-summer season. The sites in the southern part of the gradient receive a significantly higher fraction of annual precipitation as summer rain; mainly from convective storms associated with the North American Monsoon (NAM) climate system. Convective monsoon events also tend to reduce the mean daily summer atmospheric VPD for sites in the southern part of the region, especially in New Mexico and Southern Arizona (Szejner et al. 2016). The spring VPD increases from north-to-south, following the regional temperature gradient in the months prior to the onset of the NAM. The locations of all sites, along with names and three-letter reference codes are presented in Table 1.

### Regional tree response to atmospheric water demand

In this section, we discuss the primary statistical trends in the $\delta^{13}C$ and RWI chronologies from the various sites. The actual chronology data are presented in time-series, graphical form in Figs. S1 and S2 in the Supplementary Materials. The first principal component of EW $\delta^{13}C$ chronologies (PC1-EW) explained 55% of the common variance (CV) for 1960–2012 across all sites (Fig. 2, upper panels). The time series of PC1-EW was relatively stable until the final 14 years (1999–2012) when an evident trend toward a higher-than-average spring (AMJ) mean VPD values showed up (Fig. 2a, left panel). The $LW_{adj}$ $\delta^{13}C$ chronologies showed two independent local components to the common signal: one in the northwestern part of the study area, PC1-$LW_{adj,}$ explaining 28% of the CV and the other in the south/southeastern part of the study area, PC2-$LW_{adj}$, explaining 14% of the CV. The time series of the correlated, combined site variance was relatively stable across the entire 53-year span of the observations, with some weak evidence of more frequent positive deviations during the final decade (Fig. 2a, middle and right panels). When we considered all three time-series together, there was clearer evidence of recent increases in VPD for the spring (AMJ) period (i.e., in the EW correlation; PC1-EW), than for the summer (JAS) period (i.e., in the LW correlations; PC1-$LW_{adj}$ and PC2-$LW_{adj}$).

We examined the correlation between the PCA time series shown in the upper panels of Fig. 2 and the 53-year PRISM VPD time series for each 4-km grid in the geographic domain of the thirteen-site gradient. This analysis produced a broad correlation field map, allowing us to visualize the geographic extent of the three PCA-resolved regions. In other words, we determined for AMJ or JAS, separately, the spatial extent that the z-score deviations from the PCA time series were correlated with the time series of mean PRISM VPD (Fig. 2, middle panels). Grids that are shaded blue in each of the middle panels had PRISM VPD time series that were correlated with the PCA time series ($r = 0.69$, $P \leq 0.01$). The exact shade of blue was determined according to the scale of correlation coefficients shown at

the bottom of the figure. These results show that there are clear regional distinctions among the PCA-resolved correlations, and those distinctions tend to spatially track variance in PRISM-estimated VPD for spring or summer. Using the field correlations as guidance to reveal the spatial extent of each of the three PCA-defined regions, we reconstructed the PRISM-derived mean VPD time series (shown in the upper panels of Fig. 2 along with the PCA correlation time series).

We used a linear regression model of *z*-score deviations to describe for each PCA-resolved chronology, the relationship between $\delta^{13}C$ and seasonal mean VPD (Fig. 2, lower panels). The regression scatterplots show the relationship between the 53-year averaged $\delta^{13}C$ and seasonal (AMJ or JAS) PRISM VPD, for each grid in the field correlation analysis. The $\delta^{13}C$ values for PC1-EW were significantly correlated with spring VPD for all sites combined ($AMJ_{z\text{-score}} = 0.92*PC1\text{-}EW_{z\text{-score}}$ $R^2 = 0.70$, $n = 53$ years). The $\delta^{13}C$ values for PC1-$LW_{adj}$, were significantly correlated with summer VPD for 10 of the sites, mostly distributed in the northwest part of the region ($JAS_{z\text{-score}} = 0.7*PC1\text{-}LW_{z\text{-score}}$, $R^2 = 0.48$, $n = 53$ years), and $\delta^{13}C$ values for PC2-$LW_{adj}$ were correlated with summer VPD for seven of the sites, mostly in the southeastern parts of the region ($JAS_{z\text{-score}} = 0.75*PC2\text{-}LW_{z\text{-score}}$, $R^2 = 0.51$, $n = 53$ years). From these regressions, VPD variability explained between 48 and 70% of the respective EW or $LW_{adj}$ $\delta^{13}C$ variability in each selected region. The results of the regression scatterplots show evidence of a robust relationship between PRISM-modeled VPD and observed cellulose $\delta^{13}C$ across a broad climatic range and distinct seasonal precipitation regimes.

## Temporal changes tree responses to climate

Time-dependent shifts in the sensitivity of tree responses to fluctuations in wet and dry climate periods were examined on a site-by-site basis through shifts in the 30-year running average of correlations based on interannual variance (Fig. 3). We interpreted a higher correlation between interannual variance in $\delta^{13}C$ or RWI to seasonal mean VPD to be indicative of higher sensitivity of iWUE or NPP growth, respectively, to drought. Recalling the increase in drought frequency during the most recent two decades (Fig. 4, and Fig. S5 in the Electronic Supplementary Materials), we observed that following the change to higher drought frequency, the correlation coefficients and variances both increased (Fig. 3). These results showed that both $\delta^{13}C$ and RWI tracked fluctuations in 'wet' and 'dry' VPD years (from the PRISM meteorology) with higher fidelity, following the shift to greater drought frequency (see Fig. 4). All sites showed increases in the running correlation values for EW $\delta^{13}C$ with AMJ VPD, reflecting increased sensitivity to winter–spring climate. Changes in the sensitivity of EW RWI to the recent shift toward higher drought frequency were less evident compared with the $\delta^{13}C$ chronologies. Nine out of ten of the northernmost sites showed increased sensitivity in EW RWI during the past two decades. The three southernmost sites (Table 1) showed no significant changes in EW RWI sensitivity to fluctuations in winter–spring VPD.

The $LW_{adj}$ $\delta^{13}C$ chronologies, which reflect a strong response to summer VPD, showed that in three of the northernmost sites (KPP, MFP, and RCP), the running correlation values with respect to summer VPD decreased during the past two decades. The $LW_{adj}$ RWI correlations, however, at two of these sites (KPP and MFP), increased; suggesting that even at those sites with a declining, but significant, correlation between $\delta^{13}C$ and VPD, also showed increased sensitivity to drought in the RWI patterns. Correlations between $LW_{adj}$ $\delta^{13}C$ and summer VPD in the south/southeastern sites showed no significant correlation for the period before 1992, but a significant increase in correlation after 1992, once again, according to our assumptions, reflecting an increase in the sensitivity of the intrinsic water-use efficiency (iWUE) to interannual variance in summer VPD.

Decadal trends in mean seasonal VPD, as predicted by $\delta^{13}C$ chronologies, showed increases over the past 20 years, with the most evident upward trends in both frequency and calculated recurrence intervals occurring in AMJ for all sites combined and in JAS for the south/southeastern sites (Fig. 4). The probability of anomalous VPD events was observed to have increased from 0.10 per year (prior to 1992) to 0.50 per year (frequency of extreme event every 10 to 2 years before and after 1992) for AMJ precipitation (PC1-EW), and from 0.13 per year (prior to 1992) to 0.45 per year (frequency of extreme event every 7–2 years before and after 1992) for JAS precipitation (PC1-$LW_{adj}$ and PC2-$LW_{adj}$).

## Legacy effects under increasing frequency of extreme climate

Considering the 53-year time series for the non-detrended raw chronologies for all sites, we observed multiple-year legacies at most sites in both $\delta^{13}C$ and RWI (Fig. 5, upper panels). Most of the legacies lasted 2–3 years following the year of drought, though some were as long as 5 years. There was a slight tendency for longer legacies in the southernmost sites. Legacies of comparable length were observed for winter–spring and summer droughts. When the raw chronologies were detrended, the multiple-year legacies disappeared from both the $\delta^{13}C$ and RWI chronologies for most sites (Fig. 5, lower panels). For winter–spring drought at two of the northern sites (BRY and MFP for $\delta^{13}C$ of EW), legacies of 1–2 years persisted, and for summer droughts at one southern site (SLS for $\delta^{13}C$ of $LW_{adj}$) and one northern site (MFP for $\delta^{13}C$ of EW), legacies of 1 year, post-drought,

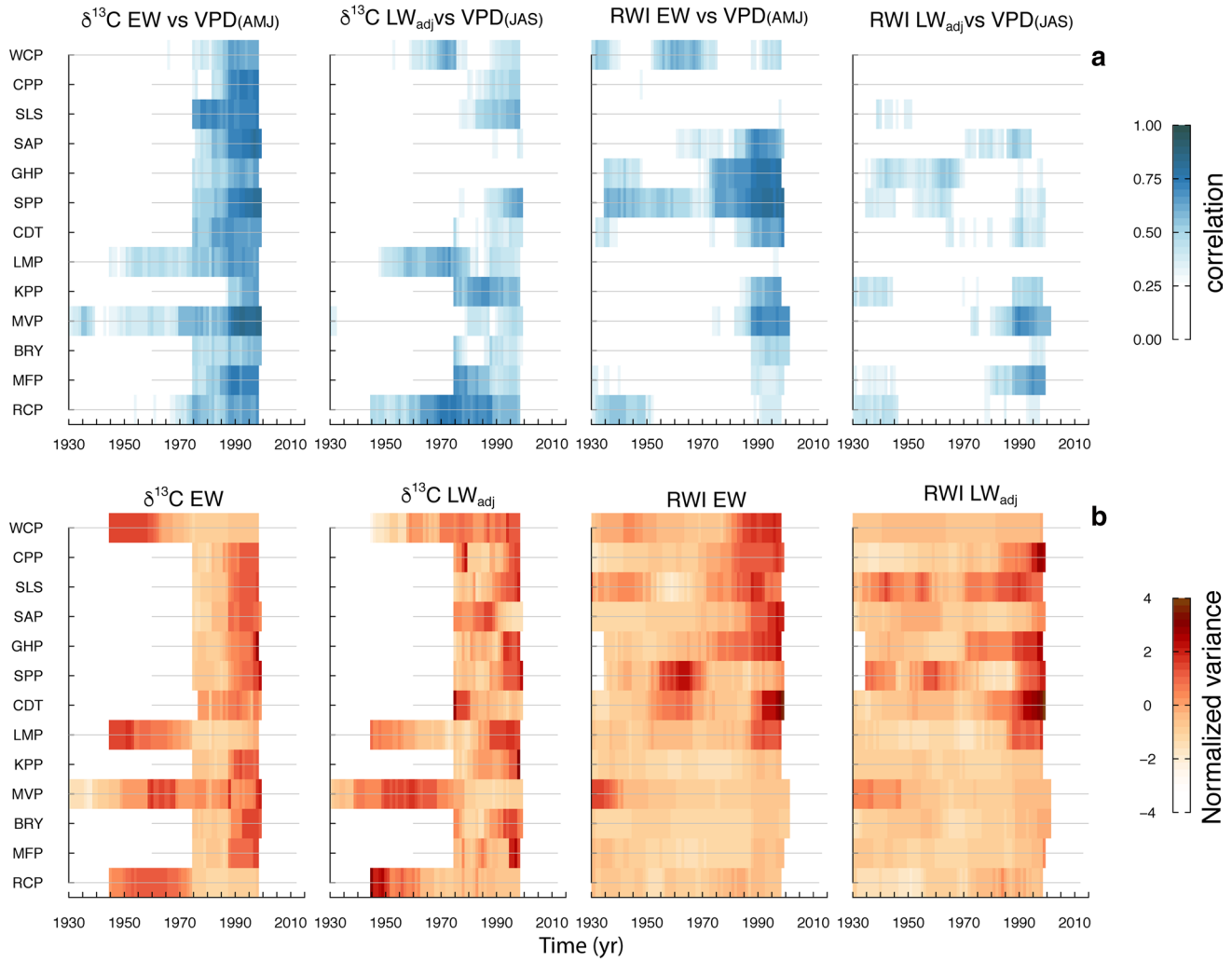


**Fig. 3** Site-specific changes in the 30-year running correlation upper panels (**a**) and variance lower panels (**b**) in the $\delta^{13}C$ and RWI responses to VPD. Vertical columns of panels are for EW or $LW_{adj}$ for either $\delta^{13}C$ or RWI. Correlation and variance color codes are centered on a 30-year moving window along the *x*-axis. For all sites (*y*-axis) concerning RWI, and three sites (WCP, LMP, and RCP) concerning $\delta^{13}C$, we analyzed 82-year chronologies (1930–2012). For one site (MVP) concerning both $\delta^{13}C$ and RWI, we analyzed a 102-year chronology (1911–2012). For all other sites for $\delta^{13}C$, we analyzed 53-year chronologies (1960–2012). Correlation values that are below alpha = 0.05 are not colored. *Y*-axes on each panel are the sites presented from south-to-north (top-to-bottom), with codes shown in the central part of the graph (color figure online)

persisted. For EW RWI, after detrending, one site MVP showed a 1-year negative growth legacy, and there was a possible 2-year negative EW RWI legacy at the LWP site, though the year of the drought showed a non-significant negative effect, suggesting a 1-year post-drought lag in the initiation of the legacy. All other sites, however, showed only effects of drought in the same year that the drought occurred, or no effects at all. For the $LW_{adj}$ RWI non-detrended raw chronologies, legacies in negative RWI responses of 3-, 4-, and even 5-years (in this case to summer rain droughts) were frequently observed in the mid- to northern-gradient sites. However, when the recent upward trend in drought frequency was removed from the chronologies, the longest observed legacies were only of 1-year duration, and then only observed at three sites (SLS, GHP, and RCP). One site (LMP) exhibited a possible 3-year negative $LW_{adj}$ RWI legacy, though the year of the drought showed a non-significant negative effect, suggesting that if a legacy effect exists, it is lagged by 1 year.

Using red-noise chronologies, we also observed significant evidence of multi-year drought legacies when the chronologies are not detrended (Fig. 5, lower panels). For the non-detrended red-noise EW $\delta^{13}C$, we observed 5-year legacies at four sites (CPP, SPP, KPP, and MVP) and 4-year legacies at two sites (SAP and GHP). When we detrended the red-noise chronologies, these legacies

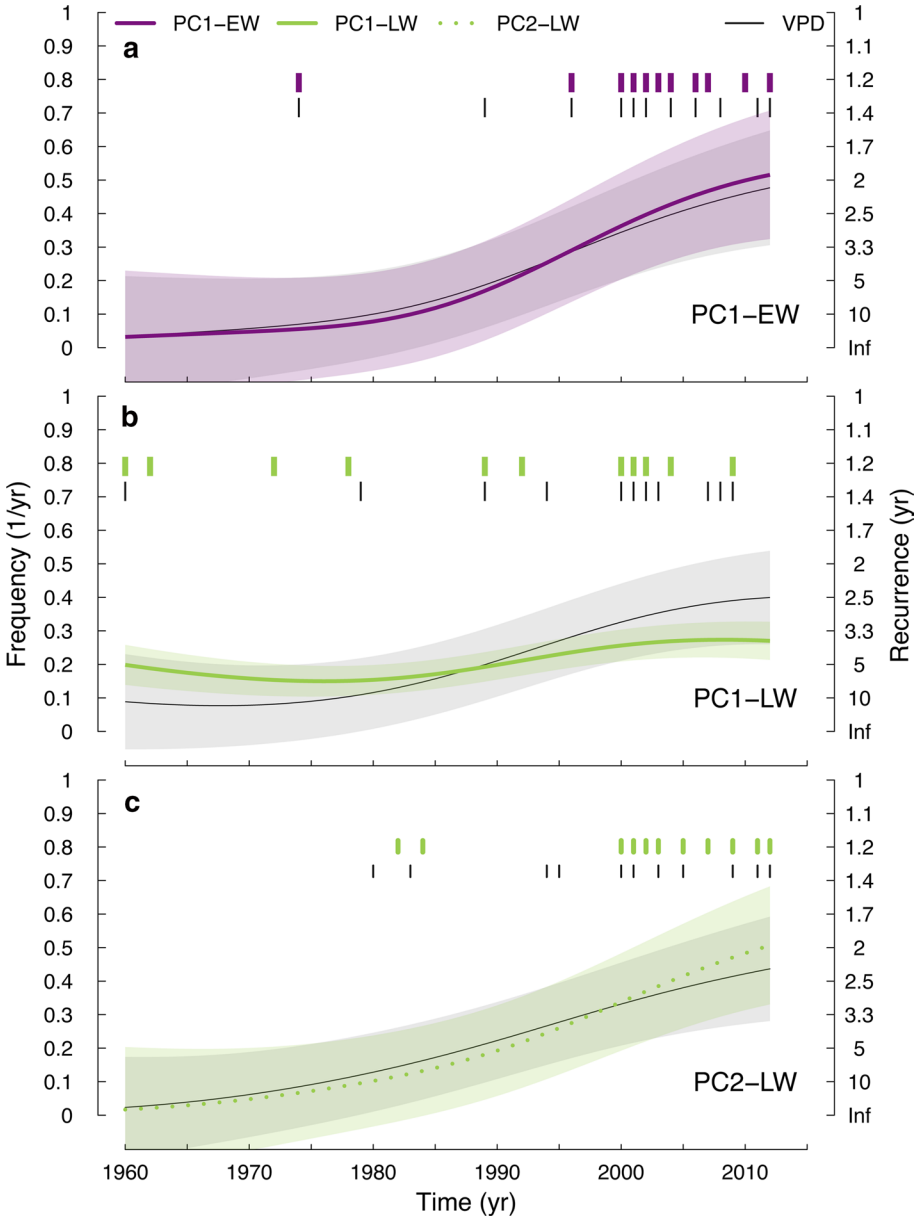


**Fig. 4** Time-dependent change in the frequency of extreme droughts based on VPD anomalies above the 80% driest seasonal periods (shown in black and derived from PRISM meteorology data) and from trends in the $\delta^{13}C$ chronologies partitioned according to the Principal Components Analysis (colored lines in each separate panel). Trends in the frequency of drought anomaly occurrence and calculated recurrence interval are shown with reference to the left and right y-axes, respectively. The frequency trend lines are shown for each of the $\delta^{13}C$ PC components, PC1-EW (**a**), PC1-$LW_{adj}$ (**b**), and PC2-$LW_{adj}$ (**c**) and confidence bands at 95% are shown as shaded envelopes (obtained from 1000 bootstrap kernel simulations) (color figure online)

decreased to reveal a 3-year legacy at only one site (MFP) and 1-year legacies at two sites (CPP and KPP). For non-detrended red-noise $LW_{adj}$ $\delta^{13}C$, we observed a 5-year legacy at one site (SLS), a 4-year legacy at one site (MVP), 3-year legacies at three sites (CDT, GHP, and SAP) and a 2-year legacy at three sites (WCP, BRY and MFP). Once detrended, we observed a single 1-year legacy (SLS) and possible 2–3 year legacies at four sites (WCP, LMP, KPP and MFP), though there was no significant influence of drought during the year of the drought in these four sites; suggesting the occurrence of a 1-year lag in producing legacy effects. Using the non-detrended red-noise chronologies for RWI, we observed weaker evidence of legacies for EW RWI, compared to EW $\delta^{13}C$ (Fig. 5, lower panels). We observed evidence for possible legacies of 4-years at one site (GHP), 2-years at one site (CDT) and 1-year at one site (SAP). In all of these cases, there was no evidence of drought influences the year of the drought, suggesting a 1-year lag in legacy effects. Once detrended, the time-series yielded evidence of a non-lagged, 1-year legacy at one site (CDT), and a possible 2-year and 1-year legacies at one site (GHP) and four sites (SLS, LMP, MVP, and RCO), respectively, if lagged by 1 year from the year of the drought. With regard to the $LW_{adj}$ RWI time series, reflecting summer droughts, we observed positive legacies, when not detrended, of 5-years at two sites (SLS and MVP), and negative legacies of 5 years at three sites (GHP, SPP, and MFP) and 4 years at one site (CDT). When one-year lags are considered, we observed the potential for legacies of 3 years at one site (KPP) and 2 years at one site (RCP).

When the chronologies were detrended to remove the effects of recent increases in drought frequency, the legacies were reduced to 1-year duration, and only observed at three sites (CPP CDT and MFP).

When all sites are considered together, and a composite picture of drought legacies for the entire network of chronologies is constructed, it is clear that observations of drought legacy length are highly influenced by drought frequencies, themselves (Fig. 6). When raw, non-detrended chronologies for both EW and $LW_{adj}$ $\delta^{13}C$ were considered, post-drought, multi-year legacies of 5-years and 2-years were observed for spring and summer droughts, respectively (using the 95% confidence intervals as guidance) (Fig. 6a). When the raw chronologies were detrended, no significant post-drought legacies were observed (Fig. 6a, lower panel). This was evident in the fact that 1 year following key drought events, $\delta^{13}C$ values (and thus iWUE) had returned to pre-drought values.

Values for EW RWI exhibited negative anomalies (indicating reduced growth) during the year of the droughts (Fig. 6b, upper panel). Values for $LW_{adj}$ RWI showed no significant anomaly with regard to mean values during or after the key drought events, though this appeared to be due to extremely large variances in the composite analysis. When the raw chronologies for EW and $LW_{adj}$ RWI were detrended, the overall variance within the composite collection of sites decreased, and a pattern of negative growth anomalies emerged for the year of key drought events, and for legacies that lasted 1–2 years following the key events (6b, lower panel).

Considering a regional picture form the network of chronologies and with the recent trend in increased drought frequency intact (without detrending). The red-noise chronologies show a weak positive effect of drought on $\delta^{13}C$ in both EW and $LW_{adj}$, but no significant effect on RWI, during the year of the event (post-drought year 0) (Fig. 6c and d, upper panels). This result was expected since the year 0 drought pattern is not dependent on interannual variance, which is the integral component of red-noise chronologies. Similar to the raw chronologies, the non-detrended red-noise chronologies of EW $\delta^{13}C$ and $LW_{adj}$ $\delta^{13}C$ showed post-drought legacies of $>5$ and 3 years, respectively (Fig. 6c, upper panel). The non-detrended red-noise chronologies for RWI showed post-drought legacies of 1–2 years for both EW and $LW_{adj}$ (Fig. 6d, upper panel). Once detrended for recent increases in drought frequency, the post-drought effects were no longer significant in EW $\delta^{13}C$ and $LW_{adj}$ $\delta^{13}C$ (Fig. 6c, lower panel). In the case of the detrended red-noise chronologies for RWI, a post-drought legacy of 1-year was observed for EW, but there was no significant legacy for $LW_{adj}$ (Fig. 6d, lower panel). These results suggest that the legacies recorded in the non-detrended, red-noise chronologies are indeed mostly explained by the increasing trend in the frequency of extreme drought conditions during the most recent two decades.

Recognizing that the result of decreasing drought legacies after detrending can be influenced by the selecting criteria of the key events used in the SEA and/or the statistical processes of the SEA itself. We reconstructed the analysis of Fig. 6 using an alternative means of choosing key events and an alternative means of assessing legacies (see Figs. S4 and S5 in the Electronic Supplementary Materials). In the case of both of these adjustments to the analysis procedure, the same result was observed—detrending the chronologies to remove the influence of recent shifts in drought frequency, substantially reduced the length of the observed legacies. In some cases, legacy lengths of 5+ years were observed without detrending, and 0–2 years, with detrending.

## Discussion

Here, we report that the temporal pattern of drought at the decadal scale has a significant and potentially profound influence on patterns of ecosystem memory and expression of legacies during drought recovery. Our observations of PRISM meteorology data, tree-ring stable isotopes and RWI have revealed evidence of a recent shift in the climate system of the southwestern US toward more frequent drought events (Fig. 4), and the tendency for that shift to produce a systematic increase in longer drought legacies (Fig. 6). Furthermore, we have sharpened the scope of past studies beyond that of annual rings alone, and their associated annual climate integrals, to show that changes in the frequency of drought are evident seasonally, occurring in both the earlywood and latewood fractions of rings. These data demonstrate that the recent shift in drought frequency has occurred for both winter and summer precipitation. Our analysis revealed up to a 50% increase in the frequency of winter–spring droughts across a broad latitudinal gradient, and a 70% increase in the frequency of summer drought in the south/southeastern part of the study region, which lies at the core of the North American Monsoon climate system. The four sites that we analyzed for 80 years (Fig. 3), extending back to 1930, showed similar increases in drought frequency during the past 20 years; providing an even more robust dendrochronological reconstruction of the recent shift in drought regime for this region (see Fig. S4 in the Electronic Supplementary Materials).

In hindsight, indirect evidence for a recent trend toward increased drought frequency in the Western U.S. has existed in past studies (Mueller et al. 2005; Anderegg et al. 2015; Schwalm et al. 2017; Serra-Maluquer et al. 2018; Peltier and Ogle 2019b). Tree-ring hydroclimate reconstructions have revealed that recent droughts in the SW, during the early 2000s, have been drier and hotter than those recorded

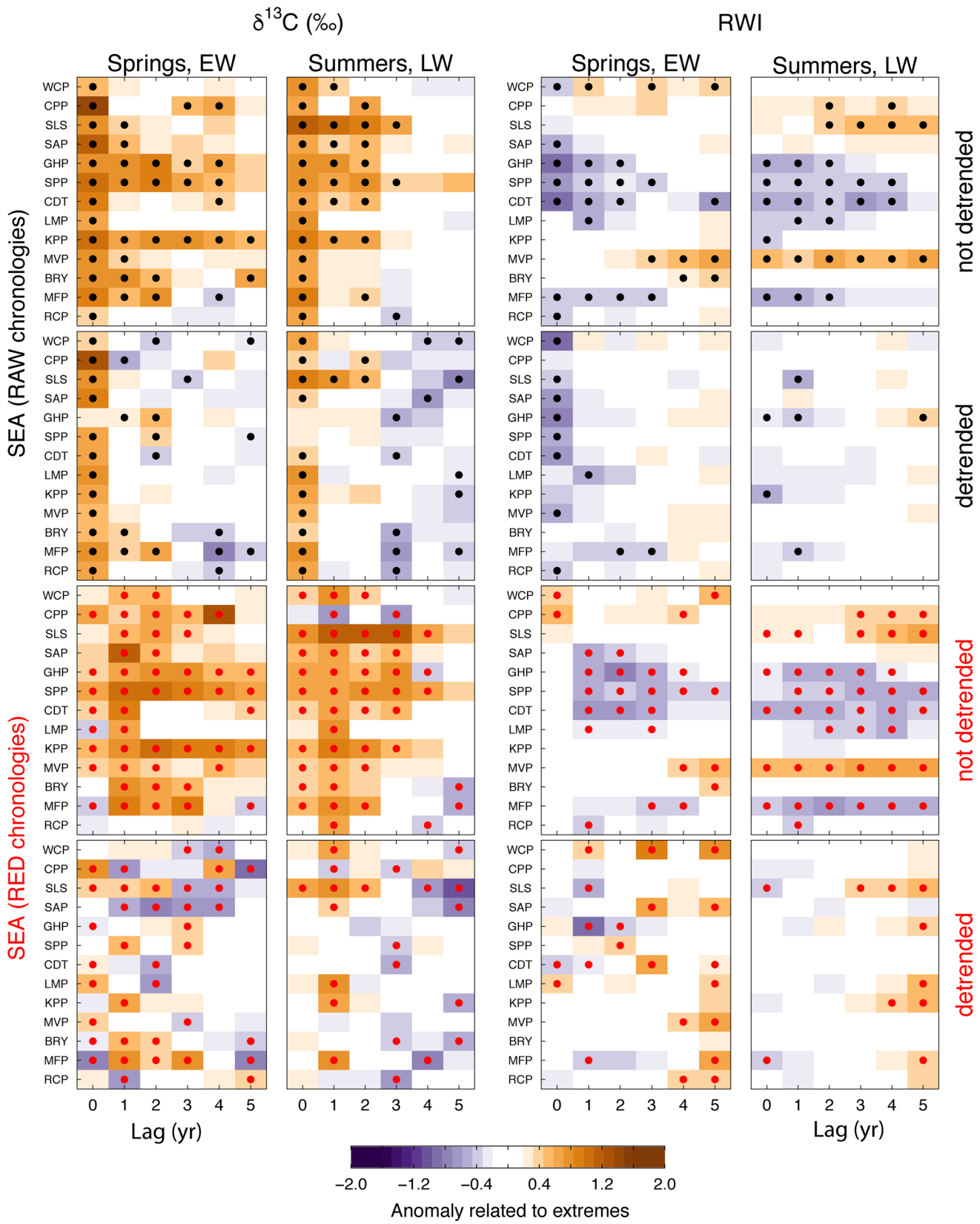
δ13C (‰)
RWI
Springs, EW
Summers, LW
Springs, EW
Summers, LW
not detrended
detrended
not detrended
detrended
SEA (RAW chronologies)
SEA (RED chronologies)
WCP
CPP
SLS
SAP
GHP
SPP
CDT
LMP
KPP
MVP
BRY
MFP
RCP
0 1 2 3 4 5
Lag (yr)
−2.0 −1.2 −0.4 0.4 1.2 2.0
Anomaly related to extremes

◂**Fig. 5** Site-based Superposed Epoch Analysis (SEA) using spring (AMJ) and summer (JAS) mean VPD. The color code represents the sign and average value of isotopic or RWI anomalies of the VPD-drought years for the 80% driest extremes at each site. Colored grids represent a significant anomaly different from a mean determined from randomly selected years and their respective legacies using a bootstrap resampling for the same number of events at each site. Colored grids reflect statistical significance to the anomalies at $P < 0.1$, and the grids with black points represent statistical significance to the anomalies at $P < 0.05$. The top two panels are the SEA for raw chronologies, either detrended or not detrended. The bottom two panels are the SEA for the red-noise chronologies, either detrended or not detrended. *x*-axis = legacy length (years). *y*-axis = sites, with codes indicated as in Table 1 (color figure online)

for the past millennium (Touchan et al. 2011). Moreover, stream flow measurements of the Colorado River since 2000 have averaged 19% below those recorded between 1906 and 1999, and have been linked to low regional snowpacks (Udall and Overpeck 2017). In support of the observational data, several modeling studies have projected increases in the frequencies of drought in the SW (Cook and Seager 2013; Ficklin and Novick 2017; Pascale et al. 2017). To our knowledge, our results are the first to show that this climatic shift is currently underway, coherent across a broad geographic area and reflected in the ecophysiological responses of forest trees.

The shift in climate regime and associated influences on $\delta^{13}C$ and RWI has a role in explaining the multi-year spans attributed to drought legacies that we observed at several sites. An increase in the frequency of droughts, by definition, shortens the intervening recovery periods between droughts. Thus, as drought frequency increases, recovery from a primary event would have a higher probability of being interrupted by a succeeding (secondary) event. This interruption reduces the probability that trees entirely "forget or bounce back" from the primary event, producing an extended legacy effect. When we initiated this study, we hypothesized that we would observe multi-year legacies at many sites, principally based on the results reported in past studies. Several studies, using annual RWI, concluded that past drought legacies in the SW, and in particular in ponderosa pine, have often lasted 4–5 years, though legacies of 2–3 years were most typical (e.g., Anderegg et al. 2015; Peltier et al. 2016; Huang et al. 2018). In fact, using raw chronologies and traditional dendrochronological detrending methods, we did indeed observe multi-year legacies. However, we found little evidence of long legacies for $\delta^{13}C$ or RWI when we accounted for the recent trend toward increased drought frequency. Once detrended, the red-noise chronologies for EW RWI only revealed a 1-year post-drought legacy (defining a legacy as being continuous with reduced growth during the year of the drought), at one of the 13 sites (Fig. 5). Four additional sites may have shown some evidence of 1-year legacies, though in these cases there was no evidence of reduced RWI growth during the year of the drought, so the post-drought legacy is disconnected from any impact during the event itself. When the $LW_{adj}$ RWI chronologies were detrended to remove the effects of recent increases in drought frequency, observed legacies were limited to 1-year duration, and only observed at three of the thirteen sites. For EW $\delta^{13}C$ chronologies, we observed a 3-year legacy at only one of the thirteen sites, and 1-year legacies at two sites (Fig. 5). When we combined responses to all key drought events from all sites using the SEA and accounted for the recent decadal-scale trend of increased drought frequency, we found no evidence of legacies in the $\delta^{13}C$ chronologies, and legacies of no longer than 1 year in the RWI chronologies (Fig. 6). Thus, overall, we did not find the same scale of previously reported multi-year legacies.

While this is a different conclusion than that revealed in past studies, it has some similarities in that it continues to indicate a potential for trees to 'remember' droughts for a limited extent of time; in this case 1–2 years when legacies are observed. Our observations provide some insight into the ecophysiological causes of legacies, when they exist. The fact that legacies were observed in the carbon isotope data, in addition to RWI, suggests a role for proximal influences, close to the short-term processes of needle $CO_2$ and $H_2O$ exchange. It is well known that high VPD has a direct influence in causing a decrease in stomatal conductance ($g_s$) in a broad array of plants (Bierhuizen and Slatyer 1965; Hall and Kaufmann 1975; Schulze et al. 1975; McAdam and Brodribb 2014; Martins et al. 2016). Stomatal guard cells are generally capable of hydro-mechanical responses to the increased evaporative demand of the atmosphere at high VPD. Reduced $g_s$, in the absence of direct feedbacks connected to $CO_2$ assimilation rate (A), will cause a reduction in the intercellular $CO_2$ concentration ($c_i$), which in turn will have an indirect influence on A. The steady-state $c_i$ at a higher VPD, generally, will be less than that at a lower VPD. A lower $c_i/c_a$ ratio will be reflected in a higher $\delta^{13}C$ ratio of sugars assimilated through photosynthesis. These interactions most likely explain our observations of higher $\delta^{13}C$ ratios in tree rings produced during drought years (e.g., Figure 6a when the lag = 0).

Drought legacies beyond the year of the drought, especially when reflected in $\delta^{13}C$, imply that information concerning the drought is retained in needles from 1 year to the next, causing the actual legacy. This information can cause persistence in reduced $g_s$, relative to A, and thus persistence of lower $c_i$ and higher $\delta^{13}C$. It is possible that these 'remembered' physiological effects are due to elevated needle concentrations of phytohormones, such as abscisic acid (ABA; Zabadal 1974; Beardsell and Cohen 1975; Brodribb and McAdam 2013; McAdam and Brodribb 2014). It is also possible that the closely spaced successive droughts extend legacies through regular boosts in leaf or needle

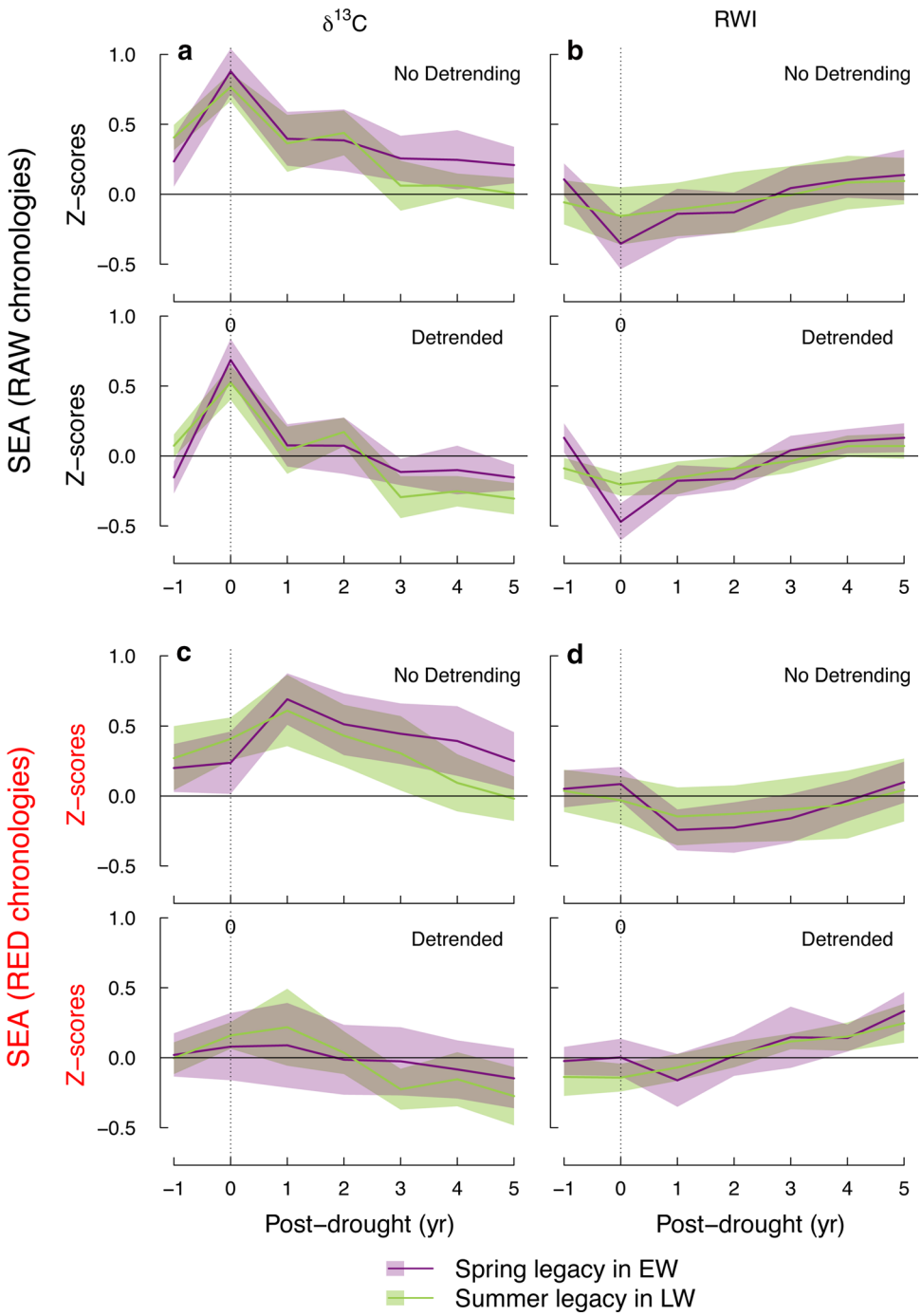


**Fig. 6** Summary trends for drought legacies recorded in EW and $LW_{adj}$ $\delta^{13}C$ and RWI. The *y*-axes show anomalies averaged for extreme events from the chronologies of $\delta^{13}C$ (**a**, **c**) and RWI (**b**, **d**). The *x*-axes represent a sequence of years prior (years < 0), during (year = 0) and after (years > 0) each extreme event identified in the SEA. "No Detrending" data include the 'raw' and 'red-noise' chronologies that retain the trend of increasing drought frequency since 1992; "Detrended" data include the 'raw' and 'red-noise' chronologies without the trend of increasing drought frequency removed. The upper four panels include chronologies that retained "random" variation (white noise). The lower four panels include chronologies from which white noise has been removed, leaving only "red-noise," which reflects interannual autocorrelations. The red- and green-colored lines and colored bands represent the average tree response and 95% confidence intervals when conducting a combined analysis of all sites "*N* = 13" treated as independent values (color figure online)

ABA concentrations. Furthermore, ABA-related memory effects could be enhanced and extended through changes in gene expression. Recent studies in citrus trees, for example, have revealed that increased leaf ABA concentrations during recurrent droughts can cause an increase in DNA methylation and associated altered gene expression (Neves et al. 2017). The ABA signal, however, has been shown to be short-lived. In most cases that have been examined, drought-induced increases in ABA levels are reversed within days-to-weeks following drought (Yan et al. 2017; Skelton et al. 2017). Thus, there is reason to search for alternative processes as potential causes of legacies. Skelton et al. (2017) provided evidence that the longest drought legacies are tied to reductions in xylem hydraulic capacity, not needle physiology, particularly in evergreen woody species. Other potential causes of drought legacies have also been hypothesized; such as those associated with reduced storage of photosynthate and associated loss of leaf (needle) area due to enhanced herbivory during the drought period (McDowell 2011). Our studies do not provide process-level insight into

these possibilities. Although, we note that we observed no evidence of thinned canopies, increased herbivory or imminent tree mortality due to carbon starvation in the trees that we studied.

The contrast between the shorter legacies observed in this study and the multi-year legacies of past studies is clear in pattern; but without explanation. Our approach to assessing legacies is different from that of previous studies, which led us to explore the possibility that the methods themselves might hold an explanation for the observed contrasts. The past studies that have reported multi-year legacies also focused on single-year droughts, or occasionally droughts of 2–3 consecutive-year durations. The key drought events that they examined were, in many cases, isolated from longer-term climate trends. This approach makes sense if one's intent is to determine the plant's ability to 'remember' past stress events. Our analysis included a broader context. It considered the composite response of 20–22 drought events and included a shifting climate regime with increased drought frequency.

To explore the potential for different analytical approaches to explain differences among the studies, we conducted additional heuristic analyses that are similar to what was used in the past. First, we developed an alternative approach to choosing key drought events; one that resulted in a more even distribution of events across the past century. To accomplish this, we removed the recent trend for increased drought frequency from the PRISM VPD chronologies at each site, and then chose our key drought events for analysis, using the 80% threshold approach described above. This resulted in a set of drought events that was not biased toward the greater drought frequencies of the most recent two decades; in essence, a set of drought events that is more evenly distributed across the 52-, 80- or 100-year tree-ring chronologies. Second, we applied a simpler 'mean differences' approach to evaluate the persistence of legacies following droughts. We computed the difference between the 5-year averaged antecedent parameter values for each key drought event, separately, and we assessed post-drought trends for lagged windows during each year immediately following the event. This is different than the SEA analysis, which compares the anomalies from each lag year with the overall average of the time series, not the antecedent values for each event separately. The latter approach, combined with a set of drought events that are more dispersed across the past century, is similar to the approaches used in past studies (e.g., Nowacki et al. 1997; Lloret et al. 2011), which have reported multi-year legacies. Whether using a distributed set of key events in combination with the mean differences approach, or the clumped distribution of events with the original SEA, the conclusion that shortened lags, or no lags, occur in chronologies detrended for the recent increases in drought frequency, remained valid. We could only replicate the conclusion of multi-year legacies in the non-detrended, raw chronologies (Fig. S6 in Electronic Supplementary Materials). In a final effort to bring alternative approaches to bear on the analysis, we applied the mean differences approach independently to drought events that occurred prior to, or after, the year 2000 (Fig. S7 in Electronic Supplementary Materials). We hypothesized that if the recent trend toward increased drought frequency was a cause of longer drought legacies, then we should see shorter legacy lengths for the decades prior to 2000, compared to those after 2000. We used only the raw chronologies for this analysis to avoid any bias due to our detrending methods. We observed no post-drought legacies for droughts prior to 2000, and multi-year legacies for droughts after 2000. In other words, it is only during the recent period of increased drought frequency that we could identify multi-year legacies. Together, these analyses strengthened our conclusion that failure to account for drought frequency causes the detection of longer drought legacies (Fig. S7). It is important to note that the shorter legacies observed in our studies were consistent across the entire spectrum of extreme droughts—from those in top 0–1% extreme-VPD bin to those in the 19–20% less extreme-VPD bin.

We cannot, even after these alternative analyses, explain why the drought legacies for events prior to 2000, which have been reported in past studies, extend for several years. It is possible that the analyses did not adequately partition the key drought events into those influenced by increased drought frequency and those not. If a combination of droughts was used in those studies, with some influenced by drought frequency, and some not, a general conclusion of multi-year lags could emerge without recognition of the nuanced influences of systematic shifts in the climate system. The Anderegg et al. (2015) study used tree-ring chronologies from the period 1948–2008, which included the first decade of the recent increase in drought frequency. They included no explicit treatment of that trend and concluded that legacies of 3–4 years are typical, especially in the SW region. The Peltier et al. (2016) study included chronologies and droughts for the 100 years ending in 2007. Thus, estimates of legacy lengths in this study may also have been affected by the recent increase in drought frequency. Even for droughts analyzed prior to the most recent decades, some of the events studied by Peltier et al. (2016) included years with closely spaced droughts, such as the period between 1984 and 1990, which included 4 analyzed drought years falling within the same 7-year period. We are not suggesting that the influences of drought frequency necessarily exclude the existence of the multi-year legacies. The legacies are clearly recorded in the tree-ring record. Rather, it may clarify the causes of the legacies; that successive droughts, closely spaced in time, may produce a synergy that results in an ecophysiological 'memory' of combined events, rather

than single events. In fact, the memory of any single event may be limited. This is a perspective that deserves further inquiry, especially given the aim of better informing prognostic models of future climate change effects.

One explanation, which carries the most promise for understanding the differences among these studies, concerns the use of different chronology databases. The past studies that have shown multi-year legacies from the SW region have relied on RWI chronologies derived from the International Tree-Ring Data Base (ITRDB) (Anderegg et al. 2015; Peltier et al. 2016, 2017; Peltier and Ogle 2019a, b; Huang et al. 2018). The ITRDB is a public archive of tree-ring data, managed by the U.S. National Center for Environmental Information and it is the most frequently used database for dendro-climate reconstructions. Recent studies, however, have revealed biases in ITRDB data (Klesse et al. 2018). Of most concern is the discovery that the ITRDB is biased toward trees that are more sensitive to climate stress. Klesse et al. (2018) showed that ITRDB samples from the SW region are biased toward sites and trees that occur at warmer and drier locations than would be representative of the region. Compared to a less biased database covering the same region (USDA Forest Inventory and Analysis, FIA), samples from the ITRDB overestimated forest climate sensitivity by 41–59%, with a bias toward greater drought effects. An analysis using both databases to predict future responses to climate change suggested that forests would respond ~ 30% less to climate extremes, when conditioned on the FIA database, compared to the ITRDB. In our studies, we chose sites and trees to explicitly avoid some of the biases in the ITRDB. Sites were chosen that are within the core range of *P. ponderosa*, rather than at the margins where abiotic stress is more likely. While we did not explicitly examine possible differences between cores from our trees and those archived in the ITRDB, it is possible, given the study by Klesse et al., that our trees experienced less frequent droughts than those in many collections of the ITRDB, especially prior to the year 2000. If so, then there is a greater likelihood that differences between our study and those in the past that report multi-year legacies are the result of more frequent and overlapping droughts reflected in the ITRDB samples. If this is indeed the cause of contrasting results among these different studies, then the differences are real; the past observations of longer, multi-year legacies and our observations of no legacies or legacies of short duration, can both be accurate, but on different sets of trees experiencing different drought frequency regimes. In that case, one question that arises is whether the past reports of long legacies accurately represent the entire region and trees that occur within their core range.

The shorter legacy effects that we describe are consistent in their absolute lengths with a recent global analysis of drought response times assessed using a random forest model conditioned on tower-flux observations, satellite remote sensing, and multi-ensemble model projections to estimate gross primary productivity (GPP) (Schwalm et al. 2017). In that study, drought recovery was estimated to be less than 12 months for 84% of the events, considering all global terrestrial regions (Schwalm et al. 2017). This analysis also revealed that the most extreme (95th and 97th percentiles) legacy periods have increased, however, from approximately 1.3 and 1.7 years, respectively, in 1901–1910, to 3 and 4.8 years, respectively, in 2001–2010, indicative of lengthening in drought legacies in recent decades. This would be consistent with our observations that drought frequency has increased in recent decades and our conclusion that this trend has increased the length of legacies.

It is also noteworthy that when we did observe legacies at specific sites, there was often a trend for slightly longer legacies in the RWI record than in the $\delta^{13}C$ record. The difference between these two metrics is small, being a 1-year average legacy observed for $\delta^{13}C$ and a 2-year average legacy for RWI. The observed legacies in both cases remain smaller than the legacies reported in past studies for RWI alone. The differences, however, might reveal corroboration of a recent study of an extreme drought in the Midwestern U.S. that showed uncoupling between the tree-ring record, which exhibited a post-drought legacy of 1 year in several tree species, and leaf-level photosynthesis or ecosystem-level GPP, which recovered relatively quickly during the same year of the drought (Kannenberg et al. 2019b).

The conclusions of our study are relevant to explaining recently observed mass-mortality events in semi-arid forests (McDowell and Allen 2015; Adams et al. 2017). McDowell et al. (2010) showed that antecedent drought stress can render trees of ponderosa pine more susceptible to mortality during subsequent droughts. Extreme drought events are likely to become even more frequent as recent model projections anticipate a 50% increase in regional mean VPD by 2100 with associated increases in forest stress and associated mortality in the Southwestern U.S. (Williams et al. 2013; McDowell and Allen 2015; Ficklin and Novick 2017). An increase in the frequency of extreme droughts, accompanied by increases in mean temperature, would provide potential synergies that amplify the probability of catastrophic mass mortality events, especially in needle-leaf forests of the southwestern US. Overall, our studies provide a climatic context for understanding forest responses to extreme drought events and an informed context within which to understand drought legacies and the hysteretic influences they impose on patterns in the global carbon budget.

**Acknowledgements** This study was supported by a grant from the Macrosystems Program in the Emerging Frontiers Section of the U.S. National Science Foundation (NSF Award 1065790), the Ecosystems Program in the Division of Environmental Biology (NSF Award 1754430), and the Inter-University Training Program in

Continental-scale Ecology (NSF Award 1137336). We thank Elisabeth Bergman, Miles Twitty, Fred Moreno, Leon Prescott Wells, Monica Vogel, Megan Mckey, Grace Kim, Alyssa Langford Abbey, and Seth Stephens for their technical assistance. Valuable discussions were provided by Valerie Trouet, Steve Leavitt, Ed Wright and Dave Meko from the Laboratory of Tree-Ring Research at the University of Arizona. The tree-ring data and isotope chronologies will be archived in the International Tree-Ring Databank or will be made available upon request to Paul Szejner (paulszejner@email.arizona.edu).

**Author contribution statement** PS and RKM conceived the ideas and designed methodology; PS, SB, and JRE collected the data; PS, SB, JRE and RKM analyzed the data; PS and RKM led the writing of the manuscript; PS, SB, JRE and RKM contributed critically to the drafts and gave final approval for publication.

**Data accessibility** All data for this manuscript will be posted in the International Tree-Ring Database (ITRDB).

## References

Adams HD, Zeppel MJB, Anderegg WRL et al (2017) A multi-species synthesis of physiological mechanisms in drought-induced tree mortality. Nat Ecol Evol 1:1285–1291. https://doi.org/10.1038/s41559-017-0248-x

Allen CD, Breshears DD, McDowell NG (2015) On underestimation of global vulnerability to tree mortality and forest die-off from hotter drought in the Anthropocene. Ecosphere. https://doi.org/10.1890/es15-00203.1

Anderegg WRL, Schwalm CR, Biondi F et al (2015) Pervasive drought legacies in forest ecosystems and their implications for carbon cycle models. Science 349:528–532. https://doi.org/10.1126/science.aab1833

Ault TR, Mankin JS, Cook BI, Smerdon JE (2016) Relative impacts of mitigation, temperature, and precipitation on 21st-Century megadrought risk in the American Southwest. Sci Adv 2:1–9. https://doi.org/10.1126/sciadv.1600873

Babst F, Alexander MR, Szejner P et al (2014) A tree-ring perspective on the terrestrial carbon cycle. Oecologia 176:307–322. https://doi.org/10.1007/s00442-014-3031-6

Barron-Gafford GA, Cable JM, Bentley LP et al (2014) Quantifying the timescales over which exogenous and endogenous conditions affect soil respiration. New Phytol 202:442–454. https://doi.org/10.1111/nph.12675

Beardsell MF, Cohen D (1975) Relationships between leaf water status, abscisic acid levels and stomatal resistance in maize and sorghum. Plant Physiol 56:207–212. https://doi.org/10.1104/pp.56.2.207

Biederman JA, Scott RL, Bell TW et al (2017) $CO_2$ exchange and evapotranspiration across dryland ecosystems of southwestern North America. Global Change Biol 23:4204–4221. https://doi.org/10.1111/gcb.13686

Bierhuizen JF, Slatyer RO (1965) Effect of atmospheric concentration of water vapour and $CO_2$ in determining transpiration photosynthesis relationships of cotton leaves. Agric Meteorol 2:259–270. https://doi.org/10.1016/0002-1571(65)90012-9

Breshears DD, Cobb NS, Rich PM et al (2005) Regional vegetation die-off in response to global-change-type drought. Proc Natl Acad Sci USA 102:15144–15148. https://doi.org/10.1073/pnas.0505734102

Brodribb TJ, McAdam SA (2013) Abscisic acid mediates a divergence in the drought response of two conifers. Plant Physiol 162:1370–1377. https://doi.org/10.1104/pp.113.217877

Bunn AG (2008) A dendrochronology program library in R (dplR). Dendrochronologia 26:115–124. https://doi.org/10.1016/j.dendro.2008.01.002

Chree C (1913) Some phenomena of sunspots and of terrestrial magnetism at Kew Observatory. Phil Trans R Soc A Math Phys Eng Sci 212:75–116. https://doi.org/10.1098/rsta.1913.0003

Cook ER, Peters K (1997) Calculating unbiased tree-ring indices for the study of climatic and environmental change. Holocene 7:361–370. https://doi.org/10.1177/095968369700700314

Cook BI, Seager R (2013) The response of the North American Monsoon to increased greenhouse gas forcing. J Geophys Res Atmos 118:1690–1699. https://doi.org/10.1002/jgrd.50111

Cook BI, Ault TR, Smerdon JE (2015) Unprecedented 21$^{st}$ Century drought risk in the American Southwest and Central Plains. Science Advances. https://doi.org/10.1126/sciadv.1400082

Dai A (2013) Increasing drought under global warming in observations and models. Nat Clim Change 3:52–58. https://doi.org/10.1038/nclimate1633

Dai A, Trenberth KE, Qian T (2004) A global dataset of Palmer Drought Severity Index for 1870–2002: relationship with soil moisture and effects of surface warming. J Hydrometeorol 5:1117–1130. https://doi.org/10.1175/JHM-386.1

Dorado-Liñán I, Piovesan G, Martínez-Sancho E et al (2019) Geographical adaptation prevails over species-specific determinism in trees' vulnerability to climate change at Mediterranean rear-edge forests. Global Change Biol 25:1296–1314. https://doi.org/10.1111/gcb.14544

Engeland K, Hisdal H, Frigessi A (2005) Practical extreme value modelling of hydrological floods and droughts: a case study. Extremes 7:5–30. https://doi.org/10.1007/s10687-004-4727-5

Farrior CE, Dybzinski R, Levin SA, Pacala SW (2013) Competition for water and light in closed-canopy forests: a tractable model of carbon allocation with implications for carbon sinks. Am Nat 181:314–330. https://doi.org/10.1086/669153

Ficklin DL, Novick KA (2017) Historic and projected changes in vapor pressure deficit suggest a continental-scale drying of the United States atmosphere. J Geophys Res Atmos 122:2061–2079. https://doi.org/10.1002/2016JD025855

Francey R, Farquhar G (1982) An explanation of $^{13}C/^{12}C$ variations in tree rings. Nature 297:28–31. https://doi.org/10.1038/297028a0

Griffin D, Meko DM, Touchan R et al (2011) Latewood chronology development for summer-moisture reconstruction in the US Southwest. Tree-Ring Res 67:87–101. https://doi.org/10.3959/2011-4.1

Hacke UG, Stiller V, Sperry JS et al (2001) Cavitation fatigue. Embolism and refilling cycles can weaken the cavitation resistance of xylem. Plant Physiol 125:779–786. https://doi.org/10.1104/pp.125.2.779

Hall AE, Kaufmann M (1975) Stomatal response to environment with *Sesamum indicum* L. Plant Physiol 55:455–459. https://doi.org/10.1104/pp.55.3.455

Hammond WM, Yu K, Wilson LA, Will RE, Anderegg WRL, Adams HD (2019) Dead or dying? Quantifying the point of no return from hydraulic failure in drought-induced tree mortality. New Phytol. https://doi.org/10.1111/nph.15922

Hartmann H, Moura C, Anderegg W, Ruehr N, Salmon Y, Allen CD, Arndt SK, Breshears DD, Davi H, Galbraith D, Ruthrof KX, Wunder J, Adams HD, Bloemen J, Cailleret M, Cobb R, Gessler A, Grams TEE, Jansen S, Kautz M, Lloret F, O'Brien M (2018) Research frontiers for improving our understanding of drought-induced tree and forest mortality. New Phytol. https://doi.org/10.1111/nph.15048

Haurwitz M, Brier G (1981) A critique of the superposed epoch analysis method—its application to solar weather relations. Mon Weather Rev 109:2074–2079. https://doi.org/10.1175/1520-0493

Huang M, Wang X, Keenan TF, Piao S (2018) Drought timing influences the legacy of tree growth recovery. Global Change Biology 24(8):3546–3559. https://doi.org/10.1111/gcb.14294

Huntington TG (2006) Evidence for intensification of the global water cycle: review and synthesis. J Hydrol 319:83–95. https://doi.org/10.1016/j.jhydrol.2005.07.003

Kannenberg SA, Maxwell JT, Pederson N, D'Orangeville L, Ficklin DL, Phillips RP (2019a) Drought legacies are dependent on water table depth, wood anatomy and drought timing across the eastern US. Ecol Lett 22:119–127. https://doi.org/10.1111/ele.13173

Kannenberg SA, Novick KA, Alexander MR, Maxwell JT, Moore DJP, Phillips RP, Anderegg WRL (2019b) Linking drought legacy effects across scales: from leaves to tree rings to ecosystems. Global Change Biol 25:2978–2992. https://doi.org/10.1111/gcb.14710

Klesse S, De Rose RJ, Guiterman CH, Lynch AM, O'Connor CD, Shaw JD, Evans MEK (2018) Sampling bias overestimates climate change impacts on forest growth in the southwestern United States. Nat Commun 9(1):5336. https://doi.org/10.1038/s41467-018-07800-y

Kolus HR, Huntzinger DN, Schwalm CR et al (2019) Land carbon models underestimate the severity and duration of drought's impact on plant productivity. Sci Rep. https://doi.org/10.1038/s41598-019-39373-1

Kozlowski TT, Pallardy SG, Kramer PJ (1991) The physiological ecology of woody plants. Academic Press, San Diego. https://doi.org/10.1016/C2009-0-02706-8

Leavitt SW, Danzer SR (1993) Method for batch processing small wood samples to holocellulose for stable-carbon isotope analysis. Anal Chem 65:87–89. https://doi.org/10.1021/ac00049a017

Lloret F, Keeling EG, Sala A (2011) Components of tree resilience: effects of successive low-growth episodes in old ponderosa pine forests. Oikos 120:1909–1920. https://doi.org/10.1111/j.1600-0706.2011.19372.x

Martins SCV, McAdam SAM, Deans RM, DaMatta FM, Brodribb TJ (2016) Stomatal dynamics are limited by leaf hydraulics in ferns and conifers: results from simultaneous measurements of liquid and vapour fluxes in leaves. Plant Cell Environ 39:694–705. https://doi.org/10.1111/pce.12668

McAdam SAM, Brodribb TJ (2014) Separating active and passive influences on stomatal control of transpiration. Plant Physiol 164:1578–1586. https://doi.org/10.1104/pp.113.231944

McCarroll D, Gagen MH, Loader NJ et al (2009) Correction of tree ring stable carbon isotope chronologies for changes in the carbon dioxide content of the atmosphere. Geochim Cosmochim Acta 73:1539–1547. https://doi.org/10.1016/j.gca.2008.11.041

McDowell NG (2011) Mechanisms linking drought, hydraulics, carbon metabolism, and vegetation mortality. Plant Physiol 155:1051–1059. https://doi.org/10.1104/pp.110.170704

McDowell NG, Allen CD (2015) Darcy's law predicts widespread forest mortality under climate warming. Nature Clim Change 5:669–672. https://doi.org/10.1038/nclimate2641

McDowell NG, Allen CD, Marshall L (2010) Growth, carbon-isotope discrimination, and drought-associated mortality across a *Pinus ponderosa* elevational transect. Global Change Biol 16:399–415. https://doi.org/10.1111/j.1365-2486.2009.01994.x

McDowell NG, Williams AP, Xu C et al (2015) Multi-scale predictions of massive conifer mortality due to chronic temperature rise. Nat Clim Change 6:295–300. https://doi.org/10.1038/nclimate2873

Meko DM, Baisan CH (2001) Pilot study of latewood-width of conifers as an indicator of variability of summer rainfall in the North American monsoon region. Int J Climatol 21:697–708. https://doi.org/10.1002/joc.646

Mekonnen ZA, Grant RF, Schwalm C (2017) Carbon sources and sinks of North America as affected by major drought events during the past 30 years. Agric For Meteorol 244–45:42–56. https://doi.org/10.1016/j.agrformet.2017.05.006

Mudelsee M, Borngen M, Tetzlaff G, Grunewald U (2003) No upward trends in the occurrence of extreme floods in central Europe. Nature 425:166–169. https://doi.org/10.1038/nature01928

Mudelsee M, Börngen M, Tetzlaff G, Grünewald U (2004) Extreme floods in central Europe over the past 500 years: role of cyclone pathway "Zugstrasse Vb". J Geophys Res Atmos 109:1–21. https://doi.org/10.1029/2004JD005034

Mueller RC, Scudder CM, Porter ME et al (2005) Differential tree mortality in response to severe drought: evidence for long-term vegetation shifts. J Ecol 93:1085–1093. https://doi.org/10.1111/j.1365-2745.2005.01042.x

Neves DM, Almeida LADH, Santana-Vieira DDS et al (2017) Recurrent water deficit causes epigenetic and hormonal changes in citrus plants. Sci Rep. https://doi.org/10.1038/s41598-017-14161-x

Novick KA, Ficklin DL, Stoy PC et al (2016) The increasing importance of atmospheric demand for ecosystem water and carbon fluxes. Nat Clim Change 6:1023–1027. https://doi.org/10.1038/NCLIMATE311

Nowacki GJ, Abrams MD, Building F (1997) Radial-growth averaging criteria for reconstructing disturbance histories from presettlement-origin oaks. Ecol Monogr 67(2):225–249

Ogle K, Whitham TG, Cobb NS (2000) Tree-ring variation in pinyon predicts likelihood of death following severe drought. Ecology 81:3237–3243. https://doi.org/10.1890/0012-9658

Ogle K, Barber JJ, Barron-Gafford GA et al (2015) Quantifying ecological memory in plant and ecosystem processes. Ecol Lett 18:221–235. https://doi.org/10.1111/ele.12399

Pascale S, Boos WR, Bordoni S et al (2017) Weakening of the North American monsoon with global warming. Nat Clim Change 7:1–8. https://doi.org/10.1038/nclimate3412

Pedersen BS (1998) The role of stress in the mortality of Midwestern oaks as indicated by growth prior to death. Ecology 79:79–93. https://doi.org/10.1890/0012-9658

Peltier DMP, Ogle K (2019a) Legacies of La Niña: North American monsoon can rescue trees from winter drought. Global Change Biol 25:121–133. https://doi.org/10.1111/gcb.14487

Peltier DMP, Ogle K (2019b) Legacies of more frequent drought in ponderosa pine across the western United States. Glob Change Biol. https://doi.org/10.1111/gcb.14720

Peltier DMP, Fell M, Ogle K (2016) Legacy effects of drought in the southwestern United States: a multi-species synthesis. Ecol Monogr 86:312–326. https://doi.org/10.1002/ecm.1219/suppinfo

Peltier DMP, Barber J, Ogle K (2017) Quantifying antecedent climatic drivers of tree growth in the Southwestern US. J Ecol 12:3218–3221. https://doi.org/10.1111/1365-2745.12878

Pettitt AN (1979) A non-parametric approach to the change-point problem. J R Stat Soc Series C (App Stat) 28:126–135. https://doi.org/10.2307/2346729

Poulter B, Frank D, Ciais P et al (2014) Contribution of semi-arid ecosystems to interannual variability of the global carbon cycle. Nature 509:600–603. https://doi.org/10.1038/nature13376

Powell TL, Galbraith DR, Christoffersen BO et al (2013) Confronting model predictions of carbon fluxes with measurements of Amazon forests subjected to experimental drought. New Phytol 200:350–365. https://doi.org/10.1111/nph.12390

Prein AF, Holland GJ, Rasmussen RM et al (2016) Running dry: the U.S. Southwest's drift into a drier climate state. Geophys Res Lett 43:1272–1279. https://doi.org/10.1002/2015GL066727

PRISM Climate Group (2004) Oregon State University. In: PRISM. http://prism.oregonstate.edu

Pugh TAM, Lindeskog M, Smith B et al (2019) The role of forest regrowth in global carbon sink dynamics. Proc Natl Acad Sci 116:1–6. https://doi.org/10.1073/pnas.1810512116

Reichstein M, Bahn M, Ciais P et al (2013) Climate extremes and the carbon cycle. Nature 500:287–295. https://doi.org/10.1038/nature12350

Schönbeck L, Gessler A, Hoch G et al (2018) Homeostatic levels of nonstructural carbohydrates after 13 year of drought and irrigation in *Pinus sylvestris*. New Phytol 219:1314–1324. https://doi.org/10.1111/nph.15224

Schulze E-D, Lange OL, Evenari M, Kappen L, Buschbom U (1975) Role of air humidity and temperature in controlling stomatal resistance of *Prunus armenica* L. under desert conditions. 3. Effect on water use efficiency. Oecologia 19:303–314. https://doi.org/10.1007/BF00348106

Schwalm CR, Anderegg WRL, Michalak AM et al (2017) Global patterns of drought recovery. Nature 548:202–205. https://doi.org/10.1038/nature23021

Seager R, Ting M, Li C et al (2013) Projections of declining surface-water availability for the southwestern United States. Nat Clim Change 3:482–486. https://doi.org/10.1038/nclimate1787

Serra-Maluquer X, Mencuccini M, Martínez-Vilalta J (2018) Changes in tree resistance, recovery and resilience across three successive extreme droughts in the northeast Iberian Peninsula. Oecologia 187:343–354. https://doi.org/10.1007/s00442-018-4118-2

Sevanto S, Mcdowell NG, Dickman LT, Pangle R, Pockman WT (2014) How do trees die? A test of the hydraulic failure and carbon starvation hypotheses. Plant Cell Environ 37(1):153–161. https://doi.org/10.1111/pce.12141

Sheffield J, Wood EF, Roderick ML (2012) Little change in global drought over the past 60 years. Nature 491:435–438. https://doi.org/10.1038/nature11575

Skelton RP, Brodribb TJ, McAdam SAM, Mitchell PJ (2017) Gas exchange recovery following natural drought is rapid unless limited by loss of leaf hydraulic conductance: evidence from an evergreen woodland. New Phytol 215:1399–1412. https://doi.org/10.1111/nph.14652

Stahle DW, Cleaveland MK, Grissino-Mayer HD et al (2009) Cool- and warm-season precipitation reconstructions over western New Mexico. J Clim 22:3729–3750. https://doi.org/10.1175/2008JCLI2752.1

Stark SC, Breshears DD, Garcia ES et al (2016) Toward accounting for ecoclimate teleconnections: intra- and inter-continental consequences of altered energy balance after vegetation change. Landsc Ecol 31:181–194. https://doi.org/10.1007/s10980-015-0282-5

Stokes MA, Smiley TL (1996) An introduction to tree-ring dating. The University of Arizona Press, Tucson, Arizona, USA. ISBN-10: 0816516804

Suess HE (1955) Radiocarbon concentration in modern wood. Science 122:415–417. https://doi.org/10.1126/science.122.3166.415-a

Szejner P, Wright WE, Babst F et al (2016) Latitudinal gradients in tree ring stable carbon and oxygen isotopes reveal differential climate influences of the North American Monsoon System. J Geophys Res Biogeosci 121:1978–1991. https://doi.org/10.1002/2016JG003460

Szejner P, Wright WE, Belmecheri S et al (2018) Disentangling seasonal and interannual legacies from inferred patterns of forest water and carbon cycling using tree-ring stable isotopes. Global Change Biol 24:5332–5347. https://doi.org/10.1111/gcb.14395

Timofeeva G, Treydte K, Bugmann H et al (2017) Long-term effects of drought on tree-ring growth and carbon isotope variability in Scots pine in a dry environment. Tree Physiol 37:1028–1041. https://doi.org/10.1093/treephys/tpx041

Touchan R, Woodhouse CA, Meko DM, Allen C (2011) Millennial precipitation reconstruction for the Jemez Mountains, New Mexico, reveals changing drought signal. Int J Climatol 31:896–906. https://doi.org/10.1002/joc.2117

Touma D, Ashfaq M, Nayak MA et al (2015) A multi-model and multi-index evaluation of drought characteristics in the 21st century. J Hydrol 526:196–207. https://doi.org/10.1016/j.jhydrol.2014.12.011

Trenberth KE, Dai A, van der Schrier G et al (2014) Global warming and changes in drought. Nat Clim Change 4:17–22. https://doi.org/10.1038/NCLIMATE2067

Udall C, Overpeck J (2017) The twenty-first century Colorado River hot drought and implications for the future. Water Resour Res 53:2404–2418. https://doi.org/10.1002/2016WR019638

Williams PA, Allen CD, Macalady AK et al (2013) Temperature as a potent driver of regional forest drought stress and tree mortality. Nat Clim Change 3:292–297. https://doi.org/10.1038/nclimate1693

Wu X, Liu H, Li X, Ciais P, Babst F, Guo W, Zhang C, Magliulo V, Pavelka M, Liu S, Huang Y, Wang P, Shi C, Ma Y (2017) Differentiating drought legacy effects on vegetation growth over the temperate Northern Hemisphere. Glob Change Biol. https://doi.org/10.1111/gcb.13920

Yan W, Zheng S, Zhong Y, Shangguan Z (2017) Contrasting dynamics of leaf potential and gas exchange during progressive drought cycles and recovery in *Amorpha fruticosa* and *Robinia pseudoacacia*. Sci Rep. https://doi.org/10.1038/s41598-017-04760-z

Yuan W, Zheng Y, Piao S, Ciais P, Lombardozzi D, Wang Y, Ryu Y et al (2019) Increased atmospheric vapor pressure deficit reduces global vegetation growth. Sci Adv. https://doi.org/10.1126/sciadv.aax1396

Zabadal TJ (1974) A water potential threshold for the increase of abscisic acid in leaves. Plant Physiol 53:125–127. https://doi.org/10.1104/pp.53.1.125